REVISION 1

The crystal structure and vibrational spectroscopy of jarosite and alunite minerals: A review

Henry J. Spratt,[1] Llew Rintoul,[1] Maxim Avdeev[2] and Wayde N. Martens[1,*]

[1]Chemistry, Physics and Mechanical Engineering, Science and Engineering Faculty, Queensland University of Technology, Brisbane, Queensland 4001, Australia

[2]Bragg Institute, Australian Nuclear Science and Technology Organisation, Lucas Heights, New South Wales 2234, Australia

*Corresponding author, email: w.martens@qut.edu.au

Abstract

The alunite supergroup of minerals are a large hydroxy-sulfate mineral group which has seen renewed interest following their discovery on Mars. Numerous reviews exist which are concerned with the nomenclature, formation and natural occurrence of this mineral group. Sulfate minerals in general are widely studied and their vibrational spectra are well characterized. However, no specific review concerning alunite and jarosite spectroscopy and crystal structure has been forthcoming. This review focuses on the controversial aspects of the crystal structure and vibrational spectroscopy of jarosite and alunite minerals. Inconsistencies regarding band assignments especially in the 1000-400 cm^{-1} region plague these two mineral groups and result in different band assignments amongst the various spectroscopic studies. There are significant crystallographic and magnetic structure

ambiguities with regards to ammonium and hydronium end members, namely, the geometry these two ions assume in the structure and the fact that hydronium jarosite is a spin glass. It was also found that the synthetic cause/s for the super cell in plumbojarosite, minamiite, huangite and walthierite are not known.

Keywords: jarosite minerals, alunite minerals, vibrational spectroscopy, Raman spectroscopy, infrared spectroscopy, crystal structure, magnetic structure, super cell

1. An introduction to the alunite supergroup of minerals

1.1 Nomenclature, formation and applications

The large alunite supergroup of minerals can be described by the general formula $AB_3(TO_4)_2(OH)_6$. The A site is most commonly occupied by a monovalent cation but divalent cations can also occupy this site. If the B site is predominantly aluminum, the mineral is classified as an alunite; if iron (III) predominates at the B site, the mineral is a jarosite. Other trivalent cations and some divalent cations can also occupy the B site. The T site is typically occupied by sulfur, but arsenic and phosphorus are common at this site as well. The alunite supergroup is further divided into subgroups based on the occupation of the T and B sites. The supergroup forms extensive solid solutions at one or all crystallographic sites, leading to a vast number of chemical formulae and possible minerals (Brophy et al., 1962; Brophy and Sheridan, 1965; Scott, 1987; Stoffregen et al., 2000). Jarosites and alunites are also able to accommodate many elements from the periodic table in their flexible crystal structure (Becker and Gasharova, 2001). However, the basic topology and structure remains the same despite the large array of potential compositions (Jambor, 1999; Stoffregen et al., 2000). This

review focuses on the jarosite (sulfur at the T site and iron at the B site) and alunite (sulfur at the T site and aluminum at the B site) subgroups. Titular jarosite and alunite, refer to the end members with potassium at the A site.

Jarosite, a mineral belonging to the alunite supergroup, was discovered on Mars at Meridiani Planum in 2004 by the Mars Exploration Rover Opportunity (Elwood Madden et al., 2004; Klingelhöfer, 2004). This discovery suggested that the Martian atmosphere was once wet and that aqueous processes occurred on Mars at some point in the planet's history. Terrestrially, jarosite type minerals are found in sulfate-rich and oxidizing environments (Baron and Palmer, 1996). Examples of these environments include: the weathering and oxidation of sulfide ore deposits and sulfide-bearing sediments, especially those of pyrite (Baron and Palmer, 1996; Becker and Gasharova, 2001; Desborough et al., 2010; Lueth et al., 2005); acid-hypersaline lake sediments (Alpers et al., 1992); the oxidation of hydrogen sulfide in epithermal areas and hot springs (Lueth et al., 2005); acid-sulfate soils (Desborough et al., 2010); and by products of metal processing industries and acid-generating mining wastes (Desborough et al., 2010; Hochella et al., 2005).

The most important application of this mineral group is the removal of iron from process solutions in the zinc, copper and lead industries (Desborough et al., 2010; Dutrizac, 2008). The supergroup could also be used for the long-term storage and immobilization of toxic and radioactive metal ions (Kolitsch and Pring, 2001). The suitability of the alunite supergroup for this purpose is due to their thermal and chemical stability. Jarosites have been shown to act as a sink for arsenic (Savage et al., 2005) and can also adsorb arsenic (Asta et al., 2009). As alunite supergroup minerals form in acidic, aqueous environments, their chemical composition can be used to place constraints on fluid conditions such as pH and Eh in the

environment (Burger et al., 2009). This review focuses on the controversial and debated aspects of the crystal structure and vibrational spectroscopy concerning the jarosite and alunite subgroups of the alunite supergroup of minerals.

1.2 Synthesis

Alunite supergroup minerals can be synthesized in a variety of ways. Hydrothermal methods using elevated temperatures and pressures (~150 °C) in a sealed vessel are the most common. Synthesis is also possible at atmospheric pressure under reflux at 100 °C. There are many reagents that can be used but essentially, a source of B site sulfate (or phosphate and arsenate depending on the composition) and a soluble form of the A site (such as nitrates, sulfates or chlorides for example) is required. Jarosites can also be prepared from the biological oxidation of Fe^{2+} to Fe^{3+} by bacteria such as *T. ferrooxidans* or the chemical oxidation of Fe^{2+} using hydrogen peroxide (Sasaki and Konno, 2000). Redox based hydrothermal methods using iron wire have also been employed (Bartlett and Nocera, 2005). It is believed that the use of chlorides at a high concentration during the synthesis of these minerals suppresses the substitution of hydronium (H_3O^+) at the A site (Basciano and Peterson, 2007b; Dutrizac, 1991). Hydronium is a common impurity due to the acidic, aqueous conditions needed for synthesis. Synthesized and natural alunite supergroup minerals are usually poorly crystalline and do not readily form single crystals (Nocera et al., 2004). Indeed, there are only a handful of single crystal diffraction studies. This has resulted in a reliance on powder based techniques for structure determination.

2. Crystal structure of the jarosite and alunite mineral subgroups

2.1 General description of the structure

The A site is 12 fold coordinate, the B site is octahedral and the T site is a distorted tetrahedron with three of the four oxygen atoms bonding to the A and B sites (Scott, 2000). The other bonds to the A and B site are from the oxygen atoms of hydroxyl groups. The apical oxygen atom from the TO_4 groups points either "up" or "down," and has a different bond length than the other three oxygen atoms (Papike et al., 2006). The crystal structure is highly symmetrical as no general positions are occupied (Papike et al., 2006). The A site is D_{3d} (3a site), the B site is C_{2h} (9d site), the TO_4 groups are C_{3v} (6c site) and the OH groups are C_s (18h site). The crystal structure can be described as alternating layers of the B site, and those comprised of A and T sites (Papike et al., 2006). This layer structure is seen more clearly when the crystal structure is projected down the *a* axis (Figure 1).

The majority of alunite supergroup minerals crystallize as the rhombohedral space group $R\bar{3}m$ (no. 166) and are described by a hexagonal axis with the number of formula units in the unit cell (Z) equal to 3 (Arkhipenko and Bokii, 1979; Papike et al., 2006). The *a* and *b* axes are identical (c.a. 7 Å) while the *c* axis is unique (c.a. 17 Å) (Stoffregen et al., 2000). Some studies have suggested that the structure could be described by the non-centrosymmetric space group R3*m* (no. 160) on the basis of pyroelectricity (Hendricks, 1937) and the detection of optical second harmonic generation (Loiacono et al., 1982). Recent measurements on a jarosite single crystal found no evidence for pyroelectricity and therefore, the space group remained centrosymmetric (Buurma et al., 2012). The overwhelming consensus in the literature is that the space group should be treated as $R\bar{3}m$. In fact, it has been recommended that all jarosites and alunites be refined as belonging to space group

125 $R\bar{3}m$ unless significant structural evidence is provided to the contrary (Menchetti and
126 Sabelli, 1976). It is well known that substitutions at the A site have the greatest effect upon
127 the *c* axis whilst substitutions at the B site influence the *a* axis the most (Basciano and
128 Peterson, 2007a; Basciano and Peterson, 2007b; Brophy et al., 1962; Brophy and Sheridan,
129 1965; Menchetti and Sabelli, 1976; Sato et al., 2009; Stoffregen et al., 2000).
130

131 **2.2 Structural variations in the supergroup: symmetry lowering**

132

133 As stated in the previous section, most alunite supergroup minerals belong to the
134 rhombohedral space group $R\bar{3}m$. However, there are a significant number of alunite
135 supergroup minerals which have been successfully refined in lower symmetry space groups.
136 Gorceixite ($BaAl_3[PO_3\ (O, OH)]_2(OH)_6$) has been observed to crystallize in the monoclinic
137 space group C*m*, but is strongly pseudorhombohedral (Blanchard, 1989; Radoslovich, 1982).
138 The lowering of symmetry from rhombohedral to monoclinic was assigned to ordered
139 protonation of one of the phosphate groups. However, a more recent investigation of the same
140 mineral determined that $R\bar{3}m$ was the most appropriate space group choice (Dzikowski et
141 al., 2006), but the authors noted that this may not be the case for all natural gorceixite
142 samples and that the mechanism for symmetry lowering is unclear. Careful analysis of
143 diffraction data and Rietveld refinement is needed to discern whether a lowering of symmetry
144 is justified.
145

146 Segnitite, $PbFe_3(AsO_4)_2(OH, H_2O)_6$, is a member of the crandallite subgroup and belongs to
147 space group $R\bar{3}m$. A segnitite related mineral with composition
148 $Pb[Zn_{0.5}\square_{0.5}]Fe_3(AsO_4)_2(OH)_6$ where □ = vacancy, was found to belong to the monoclinic

space group C2/*c* with Z = 16 (Grey et al., 2008). The basic structure was found to be similar to the normal rhombohedral structure of the alunite supergroup. However, this particular sample is unique in that there is a new site occupied: Zn is located within six membered rings formed by iron octahedra and is trigonal bipyramidal in coordination as a result of being displaced ~0.8 Å from the center of the ring. The Zn is ordered across only half of these sites and this leads to ordered displacements of Pb atoms. Ordering of partially occupied iron(III) cations and their vacancies has been attributed to a lowering of symmetry for jarosite subgroup minerals (Grey et al., 2011; Scarlett et al., 2010). In these studies, natrojarosite, titular jarosite and natrojarosite-hydronium jarosite solid solutions were prepared with ordered iron vacancies which lead to a lowering of symmetry to the monoclinic space group C2/*m*. Further study into the properties of alunite supergroup minerals with lower symmetry and not just their crystal structure, is required, especially their magnetic properties (Scarlett et al., 2010). In addition, other examples of symmetry lowered alunite supergroup minerals as a result of ordering of different atomic sites and atomic sites and their vacancies may be discovered.

2.3 Non-stoichiometry of synthesised jarosites and alunites

Most synthesized alunite supergroup minerals are not stoichiometric. The non-stoichiometry probably results from deficiencies at the A and B site rather than the T site as this makes the most structural sense (Jambor, 1999; Szymanski, 1985). Hence, the TO_4 groups are assumed to be fully occupied when calculating chemical compositions. In the majority of cases where a non-stoichiometric alunite supergroup mineral is synthesized, an excess of water/oxygen (not from OH groups) is usually observed along with an A site deficiency. This excess water is commonly attributed to the presence of the hydronium ion (H_3O^+) at the A site (Brophy

and Sheridan, 1965; Drouet and Navrotsky, 2003; Ripmeester et al., 1986; Serna et al., 1986; Stoffregen and Alpers, 1992; Stoffregen et al., 2000; Wilkins and Mateen, 1974). In addition to deficiencies at the A site, the B site is also usually not fully occupied (Basciano and Peterson, 2007b; Dutrizac and Kaiman, 1976; Nielsen et al., 2011; Nielsen et al., 2008). Vacancies at the B site of up to 30% are not uncommon. The B site vacancies are charge compensated by protonation of hydroxyl groups in the structure to form water.

The actual presence of the hydronium ion and the nature that the excess water assumes in the crystal structure is difficult to prove and has been the subject of much debate in the literature. The existence of both H_3O^+ and OH^- in the same crystal may seem surprising, especially when it is considered that H_3O^+ is surrounded by OH^- groups. It might be thought that these two groups would neutralize each other to form water molecules in the structure. Microprobe, wet chemistry and spectroscopic techniques have not conclusively shown that the hydronium ion exists in the supergroup (Stoffregen et al., 2000; Wilkins and Mateen, 1974). However, ^{1}H NMR (Ripmeester et al., 1986), ^{2}H NMR (Nielsen et al., 2011) and neutron diffraction (Wills and Harrison, 1996) studies have provided strong evidence for the presence of H_3O^+ in alunites and jarosites, and that protonation of the framework by hydronium does not occur.

2.4 Magnetic structure and proton mobility

Alunite supergroup minerals with magnetic ions such as Fe^{3+} and V^{3+} at the B site undergo long-range magnetic ordering at low temperature (Grohol et al., 2003; Matan et al., 2009). These minerals are an ideal form of the rare Kagomé lattice which is composed of magnetic ions at the corners of triangles that are connected through their vertices (Grohol et al., 2003; Matan et al., 2009; Nocera et al., 2004). For a triangular array, it is impossible for all

moments to couple antiferromagnetically and a non-collinear 120° structure is typically realized (Wills et al., 2000). In all jarosites except hydronium jarosite, long range magnetic order with the q = 0 structure is observed with a transition temperature below about 70 K (Inami et al., 2000; Matan et al., 2009; Wills et al., 2000). Hydronium jarosite on the other hand, is a spin glass with a freezing temperature at approximately 17 K (Fåk et al., 2008; Wills and Harrison, 1996; Wills et al., 1998; Wills et al., 2000). The magnetic structure is shown in Figure 2. A review on the magnetic structure of jarosite minerals has been published previously and the reader is directed there for further information (Wills, 2001).

The long range magnetic ordering has been attributed to the fact that Fe^{3+} in jarosites has a weak single-ion-type anisotropy (Inami et al., 2000). However, the cause for the spin glass behavior of hydronium jarosite is under debate. It has been proposed that hydronium jarosite is a spin glass due to: structural disorder involving hydronium, different forms of further-neighbor inter- and/or intra-plane exchange (Frunzke et al., 2001); random disorder of hydronium due to its position and/or transfer of hydrogen through the structure (Fåk et al., 2008); a more ordered FeO_6 octahedra such that the other jarosites are more disordered and have higher antiferromagnetic transition temperatures (Bisson and Wills, 2008); or the intrinsic reaction chemistry of hydronium jarosite which facilitates proton transfer from hydronium to bridging hydroxyl groups (Nocera et al., 2004), this reaction is given below in equation 1:

$$(H_3O)Fe_3(OH)_6(SO_4)_2 \rightarrow (H_3O)_{1-x}(H_2O)_xFe_3(OH)_{6-x}(H_2O)_x(SO_4)_2 \quad (1)$$

Nuclear magnetic resonance (NMR) is another method to probe magnetic structure and the spin glass behavior of hydronium jarosite. The first NMR study on hydronium alunite,

224 although undertaken to confirm the existence of hydronium in the mineral group, showed that
225 the hydronium ion has a high degree of mobility and that it is not annihilated by the
226 surrounding hydroxyl groups (Ripmeester et al., 1986). Subsequent studies have also shown
227 that the hydronium ion is highly mobile and that neutralization to water does not occur
228 (Nielsen et al., 2011; Nielsen et al., 2008). However, it has been found that there is an
229 interaction between hydronium ions and bridging hydroxyl groups from infrared
230 spectroscopy (Grohol and Nocera, 2007). Thus, the literature suggests that potential proton
231 exchange and also proton mobility are the main reasons why hydronium jarosite is a spin
232 glass, and for reasons that will be explained in the following paragraph, are linked to the
233 orientational disorder of the hydronium ion.
234
235 Ammoniojarosite, despite also having orientational disorder of the A site cation (Basciano
236 and Peterson, 2007a), shows long range magnetic order like other jarosites. In this study of
237 ammoniojarosite, the authors were able to locate the ammonium hydrogen atoms by single
238 crystal X-ray diffraction at room temperature (Basciano and Peterson, 2007a). It was found
239 that the ammonium ion is disordered across two orientations with equal probability. A
240 comparable single crystal X-ray diffraction study of hydronium jarosite, also at room
241 temperature, failed to locate the hydronium hydrogen atoms (Majzlan et al., 2004). To the
242 best of the authors' knowledge, only one study has successfully located the hydronium
243 hydrogen positions and even then, the exact geometry was said to be uncertain (Wills and
244 Harrison, 1996). Given that the pKa of H_3O^+ is 0 and the pKa of NH_4^+ is 9.25 (Atkins and De
245 Paula, 2006), it can be said that the ammonium ion is relatively unreactive with respect to the
246 surrounding hydroxyl groups when compared to the hydronium ion. It has been shown that
247 transfer of hydrogen atoms from hydronium ions to the surrounding hydroxyl groups is not
248 impossible, but if it occurs, does not result in complete neutralization to water; H_3O^+ and OH^-

249 both exist in the structure over time. Thus, it is argued that transfer of hydrogen to the
250 hydroxyl groups may be a contributing mechanism by which the dynamically disordered
251 hydronium ion reorients itself in the A site cavity. Such proton mobility would explain why
252 the hydronium hydrogen atoms are more difficult to locate by diffraction techniques when
253 compared to the ammonium hydrogen atoms, and also the observation that the hydronium ion
254 is highly mobile from NMR studies.An NMR study comparing ammonioalunite or
255 ammoniojarosite to hydronium jarosite or hydronium alunite could serve to clarify these
256 issues. To date, no NMR study of ammonioalunite or ammoniojarosite has been undertaken.
257
258 Incoherent inelastic neutron scattering (IINS) can be used to determine proton dynamics in
259 materials and has been used to assign bands to the hydronium ion for hydronium substituted
260 mordenite (Jobic et al., 1992). We are aware of only one IINS study on hydronium containing
261 alunite supergroup minerals with a view to determining proton dynamics and identifying the
262 hydronium ion. This study analyzed alunite and hydronium alunite (Lager et al., 2001) but
263 distinct peaks corresponding to hydronium were not observed. This was attributed to peaks
264 due to hydronium, hydroxyl groups and hydrogen bonded water not being to be
265 distinguished. Further IINS investigations into comparing hydronium and ammonium
266 containing jarosite or alunite minerals with their potassium counterparts are warranted.
267
268 **2.5 Structural variations in the supergroup: members with a super cell**
269
270 Despite the supergroup being largely isostructural, some members have a super cell with
271 plumbojarosite, or lead jarosite [$Pb_{0.5}Fe_3(SO_4)_2(OH)_6$], being the most well known and
272 characterized example (Hendricks, 1937; Szymanski, 1985). In this case, the super cell
273 structure is a maximal isomorphic subgroup of lowest index (Klassengleiche type IIc) of

space group $R\bar{3}m$. This means that in order for the space group and symmetry operations to be preserved when Pb^{2+} occupies the A site, the unit cell must enlarge. The super cell for plumbojarosites manifests as a doubling of the *c* axis from ~17 Å to ~34 Å (Hendricks, 1937; Szymanski, 1985). The super cell can be detected in X-ray diffraction by a peak at approximately 7 – 9 °2θ when using Cu Kα1 radiation (Jambor and Dutrizac, 1983). Additional peaks are present at higher diffraction angles, but this low angle peak is the most intense and is diagnostic of the super cell.

Other alunite supergroup minerals which possess a super cell are minamiite [(Na, Ca, K)$Al_3(SO_4)_2(OH)_6$], huangite [$Ca_{0.5}Al_3(SO_4)_2(OH)_6$] and walthierite [$Ba_{0.5}Al_3(SO_4)_2(OH)_6$] (Jambor, 1999; Ossaka et al., 1982). These minerals also have divalent cations at the A site. Thus, one might think that the presence of a divalent cation automatically results in a super cell. However, there are a number of supergroup minerals with divalent cations at the A site which have no super cell (Sato et al., 2009). Examples of these minerals include beaverite [$Pb(Fe, Cu)_3(SO_4)_2(OH)_6$], beudantite [$PbFe_3(AsO_4)(SO_4)(OH)_6$], osarizawaite [$Pb(Al, Cu)_3(SO_4)_2(OH)_6$], schlossmacherite [$(H_3O, Ca)Al_3(AsO_4, SO_4)_2(OH)_6$] and most crandallite subgroup minerals (Jambor, 1999).

As the general formula for jarosites and alunites has the A site being monovalent, a divalent cation (such as Pb^{2+}, Ca^{2+} and Ba^{2+}) at this site brings additional positive charge to the structure which must be mitigated. For those minerals which possess a super cell, charge balance is achieved by 50% occupancy of the A site. This results in two different species at the A site: the A^{2+} cation and a vacancy. When the distribution of vacancies and A^{2+} cations is ordered (repeating in a regular fashion), a super cell forms (Hendricks, 1937; Jambor,

298 1999; Jambor and Dutrizac, 1983). It has been suggested that simply ordering amongst A site
299 cations, even without the presence of vacancies, can result in a super cell (Jambor, 1999).
300
301 Such ordering of A site cations and vacancies is clearly seen for plumbojarosite (Szymanski,
302 1985). This study found that there were two different A site positions with significantly
303 different fractional occupancies with respect to lead: one with a lead occupation of 0.961
304 (termed "occupied") and one with a lead occupation of 0.039 (termed "vacant"). This
305 ordering results in alternate A sites along the *z* axis of the crystal, i.e. vacant at the Wyckoff
306 site 3a (0, 0, 0) and occupied at the Wyckoff site 3b (0, 0, ½). To account for the doubled *c*
307 axis and hence, twice as many atoms in the unit cell (Z = 6), the site symmetry of iron
308 changes to C_s and there now two crystallographically independent sulfate (6c) and hydroxyl
309 (18h) groups. Similar ordering of A site cations in minamiite was observed, such that Ca^{2+}
310 and Na^+ occupy one site whilst K^+ and Na^+ occupy the other with vacancies distributed across
311 both (Ossaka et al., 1982). The plumbojarosite structure (Szymanski, 1985) with doubled *c*
312 axis is shown in Figure 3.
313
314 A different charge balance mechanism could explain why a super cell is not observed for
315 some members of the super group despite divalent cations substituting at the A site.
316 Beaverite, beudantite, osarizawaite, schlossmacherite and the crandallite subgroup have
317 phosphorus or arsenic at the T site or a divalent cation at the B site. Hence, there is either
318 additional negative charge from the TO_4^{3-} groups or less positive charge at the B site to
319 counteract the substitution of a divalent ion at the A site. Therefore, charge balance is
320 achieved without vacancies (or another species at the A site) and subsequent ordering at the
321 A site cannot occur (a cation cannot order with itself if its site is fully occupied). Ordering of
322 cations at the A site has been previously discussed in a review (Jambor, 1999). An extensive

323 analysis of the crystal structure of various alunite and beudantite group minerals with divalent
324 cations at the A site and either divalent cations at the B site or TO_4^{3-} ions at the T site found
325 no evidence for any super cell formation (Sato et al., 2009).
326
327 However, to complicate things further, some studies have found or synthesized
328 plumbojarosite without a super cell (Bartlett and Nocera, 2005; Forray et al., 2010; Smith et
329 al., 2006). No impurities were present that could have resulted in charge balance at the T or B
330 sites in these studies. Thus, it can be said that the distribution of vacancies and lead in these
331 cases was random and not ordered. In addition, some of these studies (Forray et al., 2010;
332 Smith et al., 2006) used a synthesis route that was previously found to yield plumbojarosite
333 with a super cell (Dutrizac and Kaiman, 1976).
334
335 Given the ubiquitous presence of hydronium in the alunite supergroup, hydronium
336 substitution or chemical composition differences may be the cause of the discrepancies in *c*
337 axis length for these plumbojarosite specimens. It has been argued that the doubled *c* axis is
338 only observed in plumbojarosite when the composition approaches that of the end member
339 (Mumme and Scott, 1966). For those plumbojarosites that did not possess a doubled *c* axis,
340 hydronium at the A site would mean that these plumbojarosites were actually an intermediate
341 composition between a plumbojarosite-hydronium jarosite solid solution and ordering would
342 need to occur between three A site species (Pb^{2+}, vacancy, H_3O^+). Indeed, 74% hydronium at
343 the A site was found for one of the plumbojarosites with no doubled *c* axis (Forray et al.,
344 2010). Minamiite has ordering between three species: Ca^{2+}, Na^+ and K^+ (Ossaka et al., 1982)
345 so ordering between more than two species at the A site is not impossible. Stoichiometric
346 plumbojarosite, with respect to both Fe^{3+} and Pb^{2+}, has been prepared with no doubled *c* axis

(Bartlett and Nocera, 2005), which suggests that composition and/or hydronium content does not influence the doubling of the *c* axis in plumbojarosite.

A study of the beaverite – plumbojarosite solid solution found that *c* axis length did not correlate with composition and that a specific lead composition was not necessary to form the doubled *c* axis (Jambor and Dutrizac, 1983). Similar problems with *c* axis length have been observed for beaverite; a natural beaverite sample was found to have a doubled *c* axis while a synthetic sample did not (Hudson-Edwards et al., 2008). This was despite the natural beaverite's chemical composition not deviating significantly from the literature and other natural beaverite samples. Again, chemical composition and H_3O^+ contents do not appear to be the principle cause of *c* axis discrepancies. Therefore, it would seem that there is an unknown variable (or even variables) in the synthesis of plumbojarosite and beaverite which cause these variations in *c* axis length and the presence of a super cell. A systematic study which synthesizes plumbojarosite and beaverite under various conditions may elucidate what causes the presence or lack thereof a super cell.

The fact that in some cases the same synthesis was carried out, but different *c* axis lengths reported, suggests that the X-ray data collection and/or refinement strategies are important. Thus, all X-ray diffraction patterns should be presented (not just refined parameters) when discussing plumbojarosite and other minerals which could potentially show the effects of a super cell. Careful inspection of diffraction patterns should be undertaken so as to ascertain whether the super cell peaks are present or missing. Patterns should be collected to as low a diffraction angle as possible so the first super cell peak can be observed, as has been recommended previously (Jambor, 1999).

3. Vibrational spectroscopy of the alunite and jarosite mineral subgroups

3.1 General description of the vibrational spectra of jarosite and alunite minerals

Many extensive reviews and publications exist in the literature concerning the vibrational spectroscopy, especially that of infrared spectroscopy, for sulfate bearing minerals (Adler and Kerr, 1965; Cloutis et al., 2006; Griffith, 1970; Makreski et al., 2005; Omori and Kerr, 1963). The free sulfate ion (T_d symmetry) has $1A_1 + 1E + 2T_2$ modes of vibration. The A_1 mode is the symmetric stretch (ν_1), the doubly degenerate E mode is the deformation vibration (ν_2) whilst the T_2 modes are the triply degenerate antisymmetric stretch (ν_3) and the triply degenerate bending vibration (ν_4) (Cloutis et al., 2006). For free sulfate ions in solution, the approximate positions of these modes are 1104 cm^{-1} (ν_3), 981 cm^{-1} (ν_1), 613 cm^{-1} (ν_4) and 451 cm^{-1} (ν_2) (Adler and Kerr, 1965). These positions can be used as a general guide for the assignment of sulfate bands in vibrational spectroscopy.

The vibrational spectra of jarosites and alunites can be divided into three main groups of bands: those due to hydroxyl groups, internal modes of sulfate, and lattice modes (Chio et al., 2005; Murphy et al., 2009). Hydroxyl bands have been found to exhibit the highest sensitivity with respect to A site cation in Raman spectroscopy (Chio et al., 2010; Chio et al., 2005). The sulfate fundamental vibrations in Raman spectra, $\nu_1(SO_4)$ and $\nu_3(SO_4)$, correlate well with the *c* axis length (Sasaki et al., 1998) and in turn, the A site cation. Figures 4 and 5 are typical examples of Raman and infrared spectra of jarosites with monovalent cations at the A site.

3.2 Factor group analysis of the alunite supergroup

Factor group analysis (Adams, 1973; DeAngelis et al., 1972; Rousseau et al., 1981) is necessary to understand the vibrational spectra of solids. Factor group analysis is essentially an extension of point group symmetry principles that are applied to molecules, except solids and minerals are under analysis (Rousseau et al., 1981). Factor group analysis allows one to determine the symmetry species of all expected vibrations for the crystal of interest, assuming the chemical composition and crystal structure are known. It also facilitates accurate band assignment of vibrational spectra, especially when coupled to single crystal vibrational spectroscopic techniques (Beattie and Gilson, 1968; Damen et al., 1966). A single crystal spectroscopic study has not been performed for any member of the alunite supergroup, probably due in part to the difficulty in obtaining adequate single crystal specimens, as alluded to earlier.

The following factor group analysis was performed using the tables in Farmer (Farmer, 1974). The correlation diagram of the TO_4 groups, showing how the free (T_d) modes of vibration are affected by sitting at a lower symmetry C_{3v} site in a crystal of space group $R\bar{3}m$ (D_{3d}), is given in Table 1. The irreducible representation (total number of allowed modes), including lattice modes, is obtained after subtraction of the translational modes of the crystal ($1E_u + 1A_{2u}$) and is given by:

$\Gamma_{irred} = 8A_{1g} + 3A_{2g} + 4A_{1u} + 10A_{2u} + 11E_g + 14E_u$ (75 modes total)

Raman active modes: $8A_{1g} + 11E_g$

IR active modes: $10A_{2u} + 14E_u$

Inactive modes: $3A_{2g} + 4A_{1u}$

In the case of sulfate as the TO_4 group, Table 1 shows that: the ν_1 symmetric stretching mode (A_1) will split to give one Raman (A_{1g}) and one IR active band (A_{2u}); the ν_2 deformation mode (E) will yield one Raman (E_g) and one IR (E_u) active band; whilst the ν_3 antisymmetric stretch and the ν_4 bending vibration (both T_2) will give rise to four vibrations each ($1A_{1g}$, $1A_{2u}$, $1E_g$ and $1E_u$). Thus, at least one band from all sulfate fundamental vibrations is expected in both Raman and IR spectra. Owing to the mutual exclusion principle, the gerade (g) modes are only Raman active and the ungerade (u) modes are only IR active.

3.3 Jarosite and alunite subgroup band assignments

In most cases, the $\nu_3(SO_4)$ (1200-1000 cm^{-1}) and $\nu_4(SO_4)$ (700-600 cm^{-1}) modes should be easily assigned in infrared spectra as no other absorptions are expected in their spectral regions (Makreski et al., 2005). The $\nu_3(SO_4)$ bands are some of the strongest in the infrared spectrum (Bishop and Murad, 2005). In Raman spectra the strong band at c.a. 1000 cm^{-1} is a $\nu_1(SO_4)$ mode and the strong bands around 1100 cm^{-1} are $\nu_3(SO_4)$ modes (Chio et al., 2010; Chio et al., 2005; Makreski et al., 2005). Bands above 3000 cm^{-1} are obviously due to ν(OH) modes of vibration originating from water, hydroxyl groups and hydronium ions. There are discrepancies involving the assignment of other bands in the infrared and Raman spectra. Indeed, this mineral group has an extended lattice nature and many bands overlap in the low wavenumber region (Breitinger et al., 1997; Powers et al., 1975; Toumi and Tlili, 2008). The actual symmetry of bands in jarosite and alunite Raman and infrared spectra are yet to be assigned by a single crystal vibrational spectroscopic study. Such a study may help identify and correctly assign bands (Arkhipenko and Bokii, 1975; Damen et al., 1966; Sacuto et al., 1996).

447 An infrared band at 1640 cm^{-1} which occurs in most hydronium substituted jarosites and
448 alunites has been assigned to structural water molecules (Wilkins and Mateen, 1974). This
449 band has also been observed in all potassium-hydronium jarosite derivatives in a solid
450 solution, but the intensity of this band did not increase as the hydronium content increased
451 (Grohol and Nocera, 2007). Other studies have either assigned it to be a result of structural
452 water or surface adsorbed water (Bishop and Murad, 2005; Makreski et al., 2005; Powers et
453 al., 1975). However, it has also been argued that this band may be related to the use of KBr
454 discs to collect infrared spectra (Toumi and Tlili, 2008). This band is most likely an H–O–H
455 deformation originating from structural water, in accordance with most literature on the
456 subject. A band at ~1580 cm^{-1} has been assigned to the hydronium ion (Grohol and Nocera,
457 2007; Kubisz, 1972; Wilkins and Mateen, 1974) as its intensity decreases as the alkali metal
458 content at the A site increases (Grohol and Nocera, 2007; Wilkins and Mateen, 1974). Apart
459 from this band, there is little vibrational spectroscopic proof for the existence of hydronium at
460 the A site.
461
462 In an infrared study on alunite, jarosite and the deuterated analogue of jarosite, two bands
463 above 3000 cm^{-1} (one intense and one shoulder) were observed and assigned to ν(OH) modes
464 (Powers et al., 1975). A band at 1003 cm^{-1} was assigned to an OH deformation as it shifted to
465 761 cm^{-1} upon deuteration. Bands at 1181 and 1080 cm^{-1} were assigned to $\nu_3(SO_4)$ modes. A
466 strong band at 626 cm^{-1} and a shoulder at 650 cm^{-1} were assigned to $\nu_4(SO_4)$ modes. A weak
467 band at 1020 cm^{-1} was attributed to $\nu_1(SO_4)$. The remaining bands were attributed to lattice
468 modes and metal – oxygen vibrations. In general, band positions for alunite were higher than
469 jarosite, but no greater than 50 cm^{-1}. The $\nu_2(SO_4)$ mode went unassigned. However, this mode
470 of vibration occurs in the low wavenumber region and may have overlapped with bands due

471 to lattice modes (Bishop and Murad, 2005). For example, a $\nu_2(SO_4)$ mode was assigned to a
472 peak at 450 cm^{-1} in one infrared study (Sasaki et al., 1998).
473
474 Various jarosites with different A site cations have been studied by Raman spectroscopy
475 (Chio et al., 2010; Sasaki et al., 1998). The position and number of the sulfate fundamentals
476 were comparable, as were the lattice modes. Any minor variations in their band positions are
477 explained by expected sample variation and collection of Raman spectra as well as the
478 wavenumber cut-off at 200 cm^{-1} (Sasaki et al., 1998) and 100 cm^{-1} (Chio et al., 2010).
479 However, differences between the two studies are found in: the hydroxyl stretching region
480 with one, two or three bands being reported depending on hydronium content; a band at 1664
481 cm^{-1} which was assigned to $\nu_2(NH_4)$ (Chio et al., 2010) but not observed in the other study;
482 the number of γ(OH) modes at either two (Chio et al., 2010) or one (Sasaki et al., 1998); and
483 the presence of a δ(OH) mode at 1021 cm^{-1} (Chio et al., 2010) that went unobserved in the
484 other study.
485
486 The vibrational spectra of alunite and its deuterated analogue has been studied (Breitinger et
487 al., 1997). Four bands between 1200-1000 cm^{-1} were observed in both infrared and Raman,
488 whilst one at 1150 cm^{-1} shifted upon deuteration so it was ascribed to a δ(OH) mode. A
489 Raman band at 655 cm^{-1} did not shift upon deuteration so it was assigned to $\nu_4(SO_4)$. In the
490 infrared spectra, bands at 681, 631, 602, 529 and 432 cm^{-1} were assigned to lattice vibrations
491 involving AlO_6 octahedra as they shifted by 15 cm^{-1} upon deuteration. It was thought that
492 these bands obscure the δ(OH) and $\nu_4(SO_4)$ bands in this region, which were not assigned. An
493 infrared and Raman study on a natural alunite specimen from El Gnater, Tunisia, resulted in
494 very different band assignments in the region below 1000 cm^{-1} (Toumi and Tlili, 2008).
495

In an infrared and Raman study focused on bands due to water and hydronium, bands at 1575 and 1175 cm^{-1} were assigned to $\nu(H_3O)$ and a band at 850 cm^{-1} to H_3O rotation, but other hydronium bands were believed to be obscured by ν(OH) (Kubisz, 1972). The band at 1640 cm^{-1} was believed to be due to water which substitutes for B site cations. This study found that the infrared $\nu_1(SO_4)$ and $\nu_3(SO_4)$ bands shifted to higher wavenumber as the radius of the A site cation decreased. This study is very different to others due to more bands resulting from hydronium and water being assigned in the vibrational spectra.

Raman and infrared spectroscopy have shown that the space group for the jarosite and alunite subgroups is most likely $R\bar{3}m$ (Arkhipenko and Bokii, 1979; Serna et al., 1986), as the predicted number of bands from factor group analysis for this space group matched the observed spectra for all end members. Unlike a more recent study on ammonium jarosites and alunites (Sasaki et al., 1998), bands at both 1650 and 1430 cm^{-1} were attributed to the NH_4^+ cation in infrared spectra (Serna et al., 1986). Like other studies, there was difficulty in assigning δ(OH), γ(OH) and some sulfate fundamental modes due to overlap with metal – oxygen modes and other lattice vibrations (Serna et al., 1986). Similar band assignments and conclusions were also reached in the other study (Arkhipenko and Bokii, 1979).

3.4 Applications of jarosite and alunite vibrational spectroscopy

Given that the jarosite minerals are found on Mars, rapid identification of end members and solid solutions through vibrational spectroscopy is important. This is because compared to Mössbauer spectrometers (first used to detect jarosite minerals on Mars), vibrational spectrometers are inexpensive and handheld/portable vibrational spectrometers are available. Jarosite is stable under the surface conditions on Mars and should be able to be detected by

reflectance spectroscopy as there are diagnostic bands in the 0.4-2.5 μm region (25000-4000 cm^{-1}) (Cloutis et al., 2008). Recently, jarosite was detected in the Mawrth Vallis region of Mars through the use of orbital visible to near infrared reflectance spectroscopy (Farrand et al., 2009). Alunite, also through the use of orbital reflectance spectroscopy, has been detected on Mars at Terra Sirenum (Swayze et al., 2008). Like the earlier studies in 2004, these discoveries provide further evidence for the existence of acidic, sulfur-rich water on Mars at some point in the planet's history given the different locations where jarosite and alunite minerals have been detected.

Different jarosite type minerals themselves can be identified from other minerals in complex environments (such as mine waste and other planets) from spectroscopic measurements (Das and Hendry, 2011; Wray et al., 2011), but there are only few studies which investigate jarosite and alunite solid solutions and the effects of A, B and T site variation on vibrational spectra (Basciano and Peterson, 2007a; Basciano and Peterson, 2007b; Drouet and Navrotsky, 2003; Drouet et al., 2004). One study found that there are only subtle differences between hydronium jarosite and jarosite solid solution members with loss of detail of spectra being the only defining characteristic of hydronium content (Basciano and Peterson, 2007b). They postulated that spectroscopy may be able to determine an approximate hydronium content of jarosite minerals, including those from Mars. For instance, the lack of certain bands, those with low intensity or the comparison of intensities of two bands in the spectrum may provide an estimation of hydronium content (or other cations). Ammonium can be identified by the appearance of new bands such as an infrared band at 1423 cm^{-1} (Basciano and Peterson, 2007a). Comparing the intensity of this band with another may provide an estimation of ammonium content. A significant wavenumber decrease for the ν(OH) bands occurs when sodium occupies the A site (Drouet and Navrotsky, 2003). For jarosite-alunite

546 and natrojarosite-natroalunite solid solutions, only the position and intensity of bands change
547 (Drouet et al., 2004). Thus, the identification and rough estimation of A site cation occupancy
548 for jarosite solid solution members through vibrational spectroscopy appears promising, but
549 requires further study. Such a study may help resolve the ambiguity of band assignments in
550 the 1000-400 cm^{-1} region.
551
552 **3.5 The splitting of sulfate bands and plumbojarosite**
553
554 It has been argued that the presence of non-equivalent ions in a crystal may enrich the
555 vibrational spectrum beyond that allowed by the site symmetry (Adler and Kerr, 1965). These
556 same authors also write that the non-equivalent ions may have the same site symmetries as
557 the non-equivalency could be due to different internuclear forces as a result of changes in the
558 molecular surroundings. This is correct, and essentially what factor group analysis predicts
559 for a molecule in a crystal. They then report that three fundamental $\nu_3(SO_4)$ and $\nu_4(SO_4)$
560 bands for jarosites and alunites can be allowed in the infrared spectrum. However, factor
561 group analysis (Adams, 1973; DeAngelis et al., 1972; Rousseau et al., 1981) predicts only
562 two $\nu_3(SO_4)$ and $\nu_4(SO_4)$ modes of vibration in infrared spectra (Breitinger et al., 1997; Serna
563 et al., 1986; Toumi and Tlili, 2008). Nevertheless, assigning more sulfate fundamental modes
564 of vibration than what would normally be allowed still persists (Chio et al., 2005; Cloutis et
565 al., 2006; Murphy et al., 2009). In accordance with factor group analysis, those cases where
566 three $\nu_3(SO_4)$ bands are assigned, one of them has to be due to another vibrating unit, most
567 likely an OH deformation, given that these modes of vibration occur in similar spectral
568 regions (Sasaki et al., 1998; Serna et al., 1986).
569

570 It is correct to say that degenerate bands can split due to a lowering of symmetry, but this
571 splitting does not exceed that allowed by factor group analysis. Obviously fewer bands than
572 predicted can be observed due to resolution limitations, coincidence and overlap etc.
573 Sometimes three bands in the hydroxide stretching region are observed, despite factor group
574 analysis predicting two (Chio et al., 2010). The additional bands were explained due to the
575 extra water or hydronium that is usually present in this mineral group (Chio et al., 2010).
576
577 Plumbojarosite vibrational spectra are an interesting exception to other jarosites, as additional
578 sulfate fundamental modes of vibration are actually observed (Sasaki et al., 1998). These
579 additional bands were not observed for jarosites with a monovalent cation at the A site, and
580 hence, those with no super cell. Similar results have been reported for beaverite and
581 plumbojarosite (Hudson-Edwards et al., 2008). Figure 6 shows the Raman and infrared
582 spectra of plumbojarosite – the additional sulfate fundamental bands are clearly observed
583 when compared to Figures 3 and 4. These extra sulfate bands were attributed to the fact that
584 sulfate groups surrounding a vacancy are sufficiently different to those surrounding a Pb^{2+}
585 cation (Sasaki et al., 1998). Thus, the two different sulfate groups (one surrounding a heavy
586 Pb^{2+} ion and the other surrounding a vacancy) show the effects of additional Davydov/factor
587 group splitting when compared to jarosite and alunite minerals with no super cell.
588
589 **3.6 Symmetry problems with hydronium and ammonium ions**
590
591 As mentioned previously, hydronium is known to substitute at the A site. However, the actual
592 geometry that this ion assumes in the structure requires further investigation. Ammonium
593 (NH_4^+) is another ion that can exist at the A site. The A site has D_{3d} symmetry and therefore,
594 an inversion center. It seems surprising that H_3O^+ and NH_4^+ ions can be located at this site.

595 This is because these two ions have no inversion center and it is well known that the site
596 symmetry of a molecule must be a subgroup of the molecular symmetry (Jewess, 1982;
597 Petruševski et al., 1993; Schiebel et al., 2000); D_{3d} is not a subgroup of C_{3v} (free H_3O^+) or T_d
598 (free NH_4^+). This fact is often glossed over, and has only been mentioned in some studies
599 (Majzlan et al., 2004; Serna et al., 1986; Szymanski, 1985) with no reference to how factor
600 group analysis should be performed or vibrational spectra interpreted. If both ions are indeed
601 located at the D_{3d} site as has been shown for ammoniojarosite (Basciano and Peterson,
602 2007a), then factor group analysis cannot be performed under space group $R\bar{3}m$ with both
603 ions at the D_{3d} site due to the inversion related symmetry mismatch between the free ions and
604 the crystallographic site.
605
606 It has been suggested that H_3O^+ and NH_4^+ substitution at the A site would lower the
607 symmetry to R3*m* or another lower symmetry space group (Majzlan et al., 2004; Serna et al.,
608 1986; Szymanski, 1985). However, vibrational spectroscopic studies clearly show that the
609 spectra appear to be more in line with other jarosite and alunite minerals which are $R\bar{3}m$
610 (Serna et al., 1986). These two minerals are frequently refined in space group $R\bar{3}m$. Thus,
611 the actual geometry, and perhaps even space group, of jarosites and alunites with NH_4^+ and
612 H_3O^+ ions at the A site requires further investigation as different models and structures have
613 been proposed. For example, it has been argued based on a computational study, that the
614 hydronium ion adopts a titled configuration so that the 3-fold axis of the ion and the crystal
615 are not coincident, resulting in more potential orientations and hydrogen bonds to the
616 framework (Gale et al., 2010). An earlier study suggested that the hydronium oxygen instead
617 occupies a C_{3v} (6c) site with 50% occupancy, and hydrogen atoms at a C_s (18h) site also with

50% occupancy. (Wills and Harrison, 1996). Reconciliation of hydronium and ammoniojarosite's crystal structure with their vibrational spectra is needed.

Concluding Remarks

Despite being studied for some time, there are still many unresolved questions surrounding the alunite supergroup of minerals, in particular:

- What causes the *c* axis to be doubled in plumbojarosite, minamiite, huangite and walthierite? In addition, can the doubling of the *c* axis be controlled synthetically?
- What is the geometry of the hydronium and ammonium ions in hydronium jarosite, hydronium alunite, ammoniojarosite and ammonioalunite, and how can this be reconciled with their vibrational spectra?
- What are the symmetry species of the observed bands in Raman and infrared spectra of jarosite and alunite minerals?
- Exactly why is hydronium jarosite a spin glass? Further NMR studies comparing hydronium jarosite to ammoniojarosite would be fruitful.

There is significant overlap of bands in the low wavenumber region of jarosite and alunite vibrational spectra. As a result, lattice modes, OH deformations and some sulfate fundamental modes of vibration (in particular ν_2 and ν_4) are difficult to positively identify. Care should be taken when interpreting vibrational spectra so that more bands than allowed by factor group analysis aren't assigned; only those minerals with a super cell are expected to have additional Raman and infrared bands for sulfate fundamental modes. Deuteration

642 appears to be most useful for the alunite supergroup so that bands due to OH groups can be
643 more clearly resolved from lattice and sulfate modes of vibration.
644
645 **References Cited**
646
647 Adams, D.M. (1973) A descriptive introduction to analysis of the vibrational spectra of
648 solids. Coordination Chemistry Reviews, 10, 183-193.
649 Adler, H.H., and Kerr, P.F. (1965) Variations in infrared spectra, molecular symmetry and
650 site symmetry of sulfate minerals. American Mineralogist, 50, 132-147.
651 Alpers, C.N., Rye, R.O., Nordstrom, D.K., White, L.D., and King, B.S. (1992) Chemical,
652 crystallographic, and isotopic properties of alunite and jarosite from acid hypersaline
653 Australian lakes. Chemical Geology, 92, 203-226.
654 Arkhipenko, D.K., and Bokii, G.B. (1975) Factor group analysis and X-ray diffraction study
655 of crystals of vermiculite and talc. Journal of Structural Chemistry, 16, 417-423.
656 -. (1979) Refinement of the alunite-jarosite space group by a vibrational spectroscopic
657 method. Soviet Physics, Crystallography, 24, 100-106.
658 Asta, M.P., Cama, J., Martínez, M., and Giménez, J. (2009) Arsenic removal by goethite and
659 jarosite in acidic conditions and its environmental implications. Journal of Hazardous
660 Materials, 171, 965-972.
661 Atkins, P., and De Paula, J. (2006) Atkins' Physical Chemistry, 8th ed. Oxford University
662 Press, Oxford.
663 Baron, D., and Palmer, C.D. (1996) Solubility of jarosite at 4-35 °C. Geochimica et
664 Cosmochimica Acta, 60, 185-195.

665 Bartlett, B.M., and Nocera, D.G. (2005) Long-Range Magnetic Ordering in Iron Jarosites
666 Prepared by Redox-Based Hydrothermal Methods. Journal of the American Chemical
667 Society, 127, 8985-8993.
668 Basciano, L.C., and Peterson, R.C. (2007a) The crystal structure of ammoniojarosite,
669 $(NH_4)Fe_3(SO_4)_2(OH)_6$ and the crystal chemistry of the ammoniojarosite-hydronium
670 jarosite solid-solution series. Mineralogical Magazine, 71, 427-441.
671 -. (2007b) Jarosite-hydronium jarosite solid-solution series with full iron site occupancy:
672 mineralogy and crystal chemistry. American Mineralogist, 92, 1464-1473.
673 Beattie, I.R., and Gilson, T.R. (1968) Single crystal laser Raman spectroscopy. Proceedings
674 of the Royal Society of London. Series A, Mathematical and Physical Sciences, 307,
675 407-429.
676 Becker, U., and Gasharova, B. (2001) AFM observations and simulations of jarosite growth
677 at the molecular scale: probing the basis for the incorporation of foreign ions into
678 jarosite as a storage mineral. Physics and Chemistry of Minerals, 28, 545-556.
679 Bishop, J.L., and Murad, E. (2005) The visible and infrared spectral properties of jarosite and
680 alunite. American Mineralogist, 90, 1100-1107.
681 Bisson, W.G., and Wills, A.S. (2008) Anisotropy-driven spin glass transition in the kagome
682 antiferromagnet hydronium jarosite, $(H_3O)Fe_3(SO_4)_2(OH)_6$. Journal of Physics:
683 Condensed Matter, 20, 452204.
684 Blanchard, F.N. (1989) New X-ray powder data for gorceixite, $BaAl_3(PO_4)_2(OH_5)•H_2O$, an
685 evaluation of *d*-spacings and intensities, pseudosymmetry and its influence on the
686 figure of merit. Powder Diffraction, 4, 227-230.
687 Breitinger, D.K., Krieglstein, R., Bogner, A., Schwab, R.G., Pimpl, T.H., Mohr, J., and
688 Schukow, H. (1997) Vibrational spectra of synthetic minerals of the alunite and
689 crandallite type. Journal of Molecular Structure, 408-409, 287-290.

690 Brophy, G.P., Scott, E.S., and Snellgrove, R.A. (1962) Sulfate studies II. Solid solution
691 between alunite and jarosite. American Mineralogist, 47, 112-126.
692 Brophy, G.P., and Sheridan, M.F. (1965) Sulfate Studies IV: the jarosite-natrojarosite-
693 hydronium jarosite solid solution series. American Mineralogist, 50, 1595-1607.
694 Burger, P.V., Papike, J.J., Shearer, C.K., and Karner, J.M. (2009) Jarosite growth zoning as a
695 recorder of fluid evolution. Geochimica et Cosmochimica Acta, 73, 3248-3259.
696 Buurma, A.J.C., Handayani, I.P., Mufti, N., Blake, G.R., van Loosdrecht, P.H.M., and
697 Palstra, T.T.M. (2012) Spin-lattice coupling in iron jarosite. Journal of Solid State
698 Chemistry, 195, 50-54.
699 Chio, C.H., Sharma, S.K., Ming, L.-C., and Muenow, D.W. (2010) Raman spectroscopic
700 investigation on jarosite-yavapaiite stability. Spectrochimica Acta Part A: Molecular
701 Spectroscopy, 75, 162-171.
702 Chio, C.H., Sharma, S.K., and Muenow, D.W. (2005) Micro-Raman studies of hydrous
703 ferrous sulfates and jarosites. Spectrochimica Acta Part A: Molecular Spectroscopy,
704 61, 2428-2433.
705 Cloutis, E.A., Craig, M.A., Kruzelecky, R.V., Jamroz, W.R., Scott, A., Hawthorne, F.C., and
706 Mertzman, S.A. (2008) Spectral reflectance properties of minerals exposed to
707 simulated Mars surface conditions. Icarus, 195, 140-168.
708 Cloutis, E.A., Hawthorne, F.C., Mertzman, S.A., Krenn, K., Craig, M.A., Marcino, D.,
709 Methot, M., Strong, J., Mustard, J.F., Blaney, D.L., Bell Iii, J.F., and Vilas, F. (2006)
710 Detection and discrimination of sulfate minerals using reflectance spectroscopy.
711 Icarus, 184(1), 121-157.
712 Damen, T.C., Porto, S.P.S., and Tell, B. (1966) Raman Effect in Zinc Oxide. Physical
713 Review, 142, 570.

714 Das, S., and Hendry, M.J. (2011) Application of Raman spectroscopy to identify iron
715 minerals commonly found in mine wastes. Chemical Geology, 290, 101-108.
716 DeAngelis, B.A., Newnham, R.E., and White, W.B. (1972) Factor group analysis of the
717 vibrational spectra of crystals: a review and consolidation. American Mineralogist,
718 57, 255-268.
719 Desborough, G.A., Smith, K.S., Lowers, H.A., Swayze, G.A., Hammarstrom, H.M., Diehl,
720 S.F., Leinz, R.W., and Driscoll, R.L. (2010) Mineralogical and chemical
721 characteristics of some natural jarosites. Geochimica et Cosmochimica Acta, 74,
722 1041-1056.
723 Drouet, C., and Navrotsky, A. (2003) Synthesis, characterization, and thermochemistry of K-
724 Na-H3O jarosites. Geochimica et Cosmochimica Acta, 67, 2063-2076.
725 Drouet, C., Pass, K.L., Baron, D., Draucker, S., and Navrotsky, A. (2004) Thermochemistry
726 of jarosite-alunite and natrojarosite-natroalunite solid solutions. Geochim.
727 Cosmochim. Acta, 68(10), 2197-2205.
728 Dutrizac, J.E. (1991) The precipitation of lead jarosite from chloride media Hydrometallurgy,
729 26, 327-346.
730 Dutrizac, J.E. (2008) Factors Affecting the Precipitation of Potassium Jarosite in Sulfate and
731 Chloride Media. Metallurgical and Materials Transactions B, 39, 771-783.
732 Dutrizac, J.E., and Kaiman, S. (1976) Synthesis and properties of jarosite-type compounds
733 Canadian Mineralogist, 14, 151-158.
734 Dzikowski, T.J., Groat, L.A., and Jambor, J.L. (2006) The symmetry and crystal structure of
735 gorceixite, $BaAl_3[PO_3(O, OH)]_2(OH)_6$, a member of the alunite supergroup. Canadian
736 Mineralogist, 44, 951-958.
737 Elwood Madden, M.E., Bodnar, R.J., and Rimstidt, J.D. (2004) Jarosite as an indicator of
738 water-limited chemical weathering on Mars. Nature, 431, 821-823.

739 Fåk, B., Coomer, F.C., Harrison, A., Visser, D., and Zhitomirsky, M.E. (2008) Spin-liquid
740 behavior in a kagomé antiferromagnet: deuteronium jarosite. Europhysics Letters, 81,
741 17006.
742 Farmer, V.C., Ed. (1974) The Infrared Spectra of Minerals. Mineralogical Society, London.
743 Farrand, W.H., Glotch, T.D., Rice Jr, J.W., Hurowitz, J.A., and Swayze, G.A. (2009)
744 Discovery of jarosite within the Mawrth Vallis region of Mars: Implications for the
745 geologic history of the region. Icarus, 204, 478-488.
746 Forray, F.L., Smith, A.M.L., Drouet, C., Navrotsky, A., Wright, K., Hudson-Edwards, K.A.,
747 and Dubbin, W.E. (2010) Synthesis, characterization and thermochemistry of a Pb-
748 jarosite. Geochimica et Cosmochimica Acta, 74, 215-224.
749 Frunzke, J., Hansen, T., Harrison, A., Lord, J.S., Oakley, G.S., Visser, D., and Wills, A.S.
750 (2001) Magnetic ordering in diluted kagome antiferromagnets. Journal of Materials
751 Chemistry, 11, 179-185.
752 Gale, J.D., Wright, K., and Hudson-Edwards, K.A. (2010) A first-principles determination of
753 the orientation of H_3O^+ in hydronium alunite. American Mineralogist, 95, 1109-1112.
754 Grey, I.E., Mumme, W.G., Bordet, P., and Mills, S.J. (2008) A new crystal-chemical
755 variation of the alunite-type structure in monoclinic $PbZn_{0.5}Fe_3(AsO_4)_2(OH)_6$.
756 Canadian Mineralogist, 46, 1355-1364.
757 Grey, I.E., Scarlett, N.V.Y., Bordet, P., and Brand, H.E.A. (2011) Jarosite-butlerite
758 intergrowths in non-stoichiometric jarosites: crystal chemistry of monoclinic
759 natrojarosite-hydronium jarosite phases. Mineralogical Magazine, 75, 2775-2791.
760 Griffith, W.P. (1970) Raman studies on rock-forming minerals. Part II. Minerals containing
761 MO_3, MO_4 and MO_6 groups. Journal of the Chemical Society A, 286-291.

762 Grohol, D., Huang, Q., Toby, B.H., Lynn, J.W., Lee, Y.S., and Nocera, D.G. (2003) Powder
763 neutron diffraction analysis and magnetic structure of kagomé-type vanadium jarosite
764 $NaV_3(OD_6)(SO_4)_2$. Physical Review B, 68, 094404.
765 Grohol, D., and Nocera, D.G. (2007) Magnetic disorder in the frustrated antiferromagnet
766 jarosite arising from the H_3O^+•••OH^- interaction. Chemistry of Materials, 19(12),
767 3061-3066.
768 Hendricks, S.B. (1937) The crystal structure of alunite and the jarosites. American
769 Mineralogist, 22, 773-784.
770 Hochella, M.F., Moore, J.N., Putnis, C.V., Putnis, A., Kasama, T., and Eberl, D.D. (2005)
771 Direct observation of heavy metal-mineral association from the Clark Fork River
772 Superfund Complex: implications for metal transport and bioavailability. Geochimica
773 et Cosmochimica Acta, 69, 1651-1663.
774 Hudson-Edwards, K.A., Smith, A.M.L., Dubbin, W.E., Bennett, A.J., Murphy, P.J., and
775 Wright, K. (2008) Comparison of the structures of natural and synthetic Pb-Cu-
776 jarosite-type compounds. European Journal of Mineralogy, 20, 241-252.
777 Inami, T., Nishiyama, M., Maegawa, S., and Oka, Y. (2000) Magnetic structure of the
778 kagomé lattice antiferromagnetc potassium jarosite $KFe_3(OH)_6(SO_4)_2$. Physical
779 Review B, 61, 12181-12186.
780 Jambor, J.L. (1999) Nomenclature of the alunite supergroup. Canadian Mineralogist, 37,
781 1323-1341.
782 Jambor, J.L., and Dutrizac, J.E. (1983) Beaverite-plumbojarosite solid solutions. Canadian
783 Mineralogist, 21, 101-113.
784 Jewess, M. (1982) A theoretical treatment of 'orientational' disorder for routine use. Acta
785 Crystallographer B, 38, 1418-1422.

786 Jobic, H., Czjzek, M., and Van Santen, R.A. (1992) Interaction of water with hydroxyl
787 groups in H-mordenite: a neutron inelastic scattering study. Journal of Physical
788 Chemistry, 96, 1540-1542.
789 Klingelhöfer, G.M., R. V.; Bernhardt, B.; Schröder, C.; Rodionov, D. S.; de Souza Jr, P. A.;
790 Yen, A.; Gellert, R.; Evlanov, E. N.; Zubkov, B.; Foh, J.; Bonnes, U.; Kankeleit, E.;
791 Gütlich, P.; Ming, D. W.; Renz, F.; Wdowiak, T.; Squyres, S. W.; Arvidson, R. E.
792 (2004) Jarosite and hematite at Meridiani Planum from Opportunity's Mossbauer
793 spectrometer. Science, 306, 1740-1745.
794 Kolitsch, U., and Pring, A. (2001) Crystal chemistry of the crandallite, beudantite and alunite
795 groups: a review and evaluation of the suitability as storage materials for toxic metals.
796 Journal of Mineralogical and Petrological Sciences, 96, 67-78.
797 Kubisz, J. (1972) Studies on synthetic alkali-hydronium jarosites III: infrared absorption
798 study. Mineralogia Polonica, 3, 23-37.
799 Lager, G.A., Swayze, G.A., Loong, C.-K., Rotella, F.J., Richardson, J.W., and Stoffregen,
800 R.E. (2001) Neutron spectroscopic study of synthetic alunite and oxonium-substituted
801 alunite. Canadian Mineralogist, 39, 1131-1138.
802 Loiacono, G.M., Kostecky, G., and White, J.S. (1982) Resolution of space group ambiguities
803 in minerals. American Mineralogist, 67, 846-847.
804 Lueth, V.W., Rye, R.O., and Peters, L. (2005) “Sour gas” hydrothermal jarosite: ancient to
805 modern acid-sulfate mineralization in the southern Rio Grande Rift. Chemical
806 Geology, 215, 339-360.
807 Majzlan, J., Stevens, R., Boerio-Goates, J., Woodfield, B.F., Navrotsky, A., Burns, P.C.,
808 Crawford, M.K., and Amos, T.G. (2004) Thermodynamic properties, low-temperature
809 heat-capacity anomalies, and single-crystal X-ray refinement of hydronium jarosite,
810 $(H_3O)Fe_3(SO_4)_2(OH)_6$. Physics and Chemistry of Minerals, 31, 518-531.

811 Makreski, P., Jovanoski, G., and Dimitrovska, S. (2005) Minerals from Macedonia XIV.
812 Identification of some sulfate minerals by vibrational (infrared and Raman)
813 spectroscopy. Vibrational Spectroscopy, 39, 229-239.
814 Matan, K., Helton, J.S., Grohol, D., Nocera, D.G., Wakimoto, S., Kakurai, K., and Lee, Y.S.
815 (2009) Polarized neutron scattering studies of the kagomé lattice antiferromagnet
816 $KFe_3(OH)_6(SO_4)_2$. Physica B, 404, 2529-2531.
817 Menchetti, S., and Sabelli, C. (1976) Crystal chemistry of the alunite series: crystal structure
818 refinement of alunite and synthetic jarosite. Neues Jahrbuch für Mineralogie
819 Monatshefte, 9, 406-417.
820 Mumme, W.G., and Scott, T.R. (1966) The relationship between basic ferric sulfate and
821 plumbojarosite. American Mineralogist, 51, 443-453.
822 Murphy, P.J., Smith, A.M.L., Hudson-Edwards, K.A., Dubbin, W.E., and Wright, K. (2009)
823 Raman and IR Spectroscopic Studies of Alunite-Supergroup Compounds Containing,
824 Al^{3+}, Cr^{3+} Fe^{3+} and V^{3+} at the B Site. Canadian Mineralogist, 47, 663-681.
825 Nielsen, U.G., Heinmaa, I., Samoson, A., Majzlan, J., and Grey, C.P. (2011) Insight into the
826 local magnetic environments and deuteron mobility in jarosite
827 $(AFe_2(SO_4)_2(OD,OD_2)_6$, A = K, Na, $D_3O)$ and hydronium alunite
828 $((D_3O)Al_3(SO_4)_2(OD)_6)$, from variable-temperature ^2H MAS NMR spectroscopy.
829 Chemistry of Materials, 23, 3176-3187.
830 Nielsen, U.G., Majzlan, J., and Grey, C.P. (2008) Determination and quantification of the
831 local environments in stoichiometric and defect jarosite by solid-state ^2H NMR
832 spectroscopy. Chemistry of Materials, 20, 2234-2241.
833 Nocera, D.G., Bartlett, B.M., Grohol, D., Papoutsakis, D., and Shores, M.P. (2004) Spin
834 frustration in 2D kagomé lattices: a problem for inorganic synthetic chemistry.
835 Chemistry a European Journal, 10, 3850-3859.

836 Omori, K., and Kerr, P.F. (1963) Infrared Studies of Saline Sulfate Minerals. Geological
837 Society of America Bulletin, 74, 709-734.
838 Ossaka, J., Hirabayashi, J.-I., Okada, K., and Kobayashi, R. (1982) Crystal structure of
839 minamiite, a new mineral of the alunite group. American Mineralogist, 67, 114-119.
840 Papike, J.J., Karner, J.M., and Shearer, C.K. (2006) Comparative planetary mineralogy:
841 Implications of martian and terrestrial jarosite. A crystal chemical perspective.
842 Geochimica et Cosmochimica Acta, 70, 1309-1321.
843 Petruševski, V.M., Minčeva-Šukarova, B., and Džorovska, A. (1993) The vibrational species
844 of molecules in disordered crystals: $M(NH_3)_2$ groups at C_{4h} symmetry sites. Bulletin
845 of the Chemists and Technologists of Macedonia, 12, 31-34.
846 Powers, D.A., Rossman, G.R., Schugar, H.J., and Gray, H.B. (1975) Magnetic behavior and
847 infrared spectra of jarosite, basic iron sulfate and their chromate analogies. Journal of
848 Solid State Chemistry, 13, 1-13.
849 Radoslovich, E.W. (1982) Refinement of gorceixite in C*m*. Neues Jahrbuch für Mineralogie
850 Monatshefte, 446-464.
851 Ripmeester, J.A., Ratcliffe, C.I., Dutrizac, J.E., and Jambor, J.L. (1986) Hydronium ion in the
852 alunite - jarosite group. Canadian Mineralogist, 24, 435-447.
853 Rousseau, D.L., Bauman, R.P., and Porto, S.P.S. (1981) Normal mode determination in
854 crystals. Journal of Raman Spectroscopy, 10, 253-290.
855 Sacuto, A., Lebon, A., Colson, D., Bertinotti, A., Marucco, J.F., and Viallet, V. (1996)
856 Normal-modes study of $HgBa_2Ca_2Cu_3O_8^+$[delta] single crystals by a micro-Raman
857 analysis. Physica C, 259, 209-217.
858 Sasaki, K., and Konno, H. (2000) Morphology of jarosite-group compounds precipitated from
859 biologically and chemically oxidized Fe ions. Canadian Mineralogist, 38, 45-56.

Sasaki, K., Tanaike, O., and Konno, H. (1998) Distinction of jarosite-group compounds by Raman spectroscopy. Canadian Mineralogist, 36, 1225-1235.

Sato, E., Nakai, I., Miyawaki, R., and Matsubara, S. (2009) Crystal structures of alunite family minerals: beaverite, corkite, alunite, natroalunite, jarosite, svanbergite, and woodhouseite. Neues Jahrbuch für Mineralogie Abhandlungen, 185, 313-322.

Savage, K.S., Bird, D.K., and O'Day, P.A. (2005) Arsenic speciation in synthetic jarosite. Chemical Geology, 215, 473-498.

Scarlett, N.V.Y., Grey, I.E., and Brand, H.E.A. (2010) Ordering of iron vacancies in monoclinic jarosites. American Mineralogist, 95, 1590-1593.

Schiebel, P., Burger, K., Büttner, H.G., Kearley, G.J., Lehmann, M., and Prandl, W. (2000) ND_3-Density distribution in orientationally disordered $Ni(ND_3)_6Cl_2$ observed by means of neutron Laue diffraction. Journal of Physics: Condensed Matter, 12, 8567-8576.

Scott, K.M. (1987) Solid solution in, and classification of, gossan-derived members of the alunite-jarosite family, northwest Queensland, Australia. American Mineralogist, 72, 178-187.

Scott, K.M. (2000) Nomenclature of the alunite supergroup: Discussion. Canadian Mineralogist, 38(5), 1295-1297.

Serna, C.J., Cortina, C.P., and Garcia Ramos, J.V. (1986) Infrared and Raman study of alunite-jarosite compounds. Spectrochimica Acta Part A: Molecular Spectroscopy, 42A, 729-734.

Smith, A.M.L., Dubbin, W.E., Wright, K., and Hudson-Edwards, K.A. (2006) Dissolution of lead- and lead-arsenic-jarosites at pH 2 and 8 and 20 °C: Insights from batch experiments. Chemical Geology, 229, 344-361.

884 Stoffregen, R.E., and Alpers, C.N. (1992) Observations on the unit-cell dimensions, H_2O
885 contents and δD values of natural and synthetic alunite. American Mineralogist, 77,
886 1092-1098.
887 Stoffregen, R.E., Alpers, C.N., and Jambor, J.L. (2000) Alunite-jarosite crystallography,
888 thermodynamics, and geochronology. Reviews in Mineralogy and Geochemistry, 40,
889 453-479.
890 Swayze, G.A., Ehlmann, B.L., Milliken, R.E., Poulet, F., Wray, J.J., Rye, R.O., Clark, R.N.,
891 Desborough, G.A., Crowley, J.K., Gondet, B., Mustard, J.F., Seelos, K.D., Murchie,
892 S.L., and the MRO CRISM team. (2008) Discovery of the acid-sulfate mineral alunite
893 in Terra Sirenum, Mars, using MRO CRISM: possible evidence for acid-saline
894 lacustrine deposits? American Geophysical Union, Fall Meeting 2008, Abstract
895 #P44A-04.
896 Szymanski, J.T. (1985) The crystal structure of plumbojarosite. Canadian Mineralogist, 23,
897 659-668.
898 Toumi, M., and Tlili, A. (2008) Rietveld Refinement and Vibrational Spectroscopic Study of
899 Alunite from El Gnater, Central Tunisia. Russian Journal of Inorganic Chemistry, 53,
900 1845.
901 Wilkins, R.W.T., and Mateen, A. (1974) The spectroscopic study of oxonium ions in
902 minerals. American Mineralogist, 59, 811-819.
903 Wills, A.S. (2001) Conventional and unconventional orderings in the jarosites. Canadian
904 Journal of Physics, 79, 1501-1510.
905 Wills, A.S., and Harrison, A. (1996) Structure and magnetism of hydronium jarosite, a model
906 Kagomé antiferromagnet. Journal of the Chemical Society, Faraday Transactions, 92,
907 2161-2166.

Wills, A.S., Harrison, A., Mentink, S.A.M., Mason, T.E., and Tun, Z. (1998) Magnetic correlations in deuteronium jarosite, a model S = 5/2 Kagomé antiferromagnet. Europhysics Letters, 42, 325-330.

Wills, A.S., Harrison, A., Ritter, C., and Smith, R.I. (2000) Magnetic properties of pure and diamagnetically doped jarosites: model kagomé antiferromagnets with variable coverage of the magnetic lattice. Physical Review B, 61, 6156-6169.

Wray, J.J., Milliken, R.E., Dundas, C.M., Swayze, G.A., Andrews-Hanna, J.C., Baldridge, A.M., Chojnacki, M., Bishop, J.L., Ehlmann, B.L., Murchie, S.L., Clark, R.N., Seelos, F.P., Tornabene, L.L., and Squyres, S.W. (2011) Columbus crater and other possible groundwater-fed paleolakes of Terra Sirenum, Mars. Journal of Geophysical Research, 116, E01001.

List of Figure Captions

Figure 1. The crystal structure of jarosite projected down the *a* axis showing sulfate tetrahedra and FeO_6 octahedra.

Figure 2. Magnetic structure of jarosites showing a) the impossibility of all moments coupling antiferromagnetically in a triangular array, b) one of the many degenerate ground states that is obtained by rotating the moments 120 ° and c) the q = 0 array of magnetic moments that is at T < 70 K. Adapted from Wills and Harrison (1996).

Figure 3. The crystal structure of super cell plumbojarosite projected down the *a* axis showing SO_4 and FeO_6 as polyhedra.

933 Figure 4. Typical Raman spectrum of jarosite [$KFe_3(SO_4)_2(OH)_6$].

934

935 Figure 5. Typical infrared spectrum of jarosite [$KFe_3(SO_4)_2(OH)_6$].

936

937 Figure 6. Raman and infrared spectra of super cell plumbojarosite from 900 – 1300 cm^{-1}.

938

939 **Tables**

940

941 Table 1. Factor group splitting of the internal modes for TO_4 groups

Molecular symmetry (T_d)	Site symmetry (C_{3v})	Crystal symmetry (D_{3d})
A_1	$3A_1$	$3A_{1g}$ (Raman active)
		$3A_{2u}$ (IR active)
E	3E	$3E_g$ (Raman active)
		$3E_u$ (IR activce)
$2T_2$		

942

943 **Figures**

944

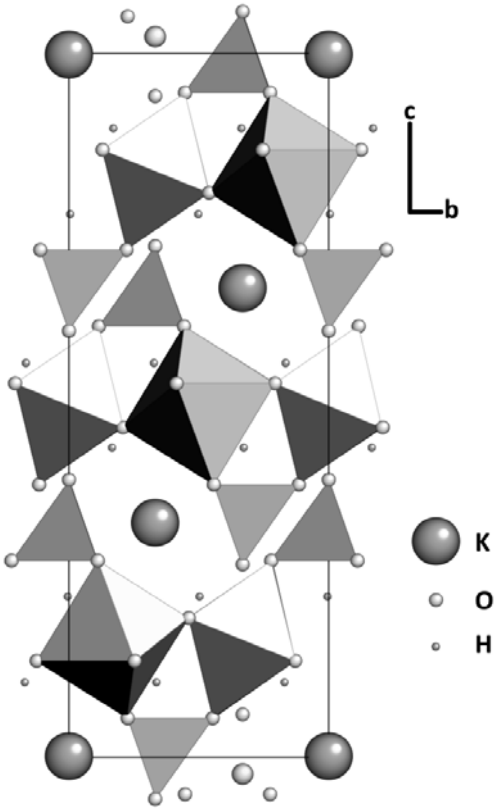

945

946 Fig. 1

947

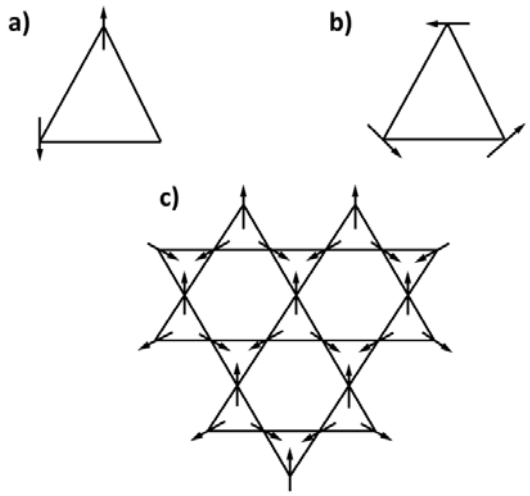

948

949 Fig. 2

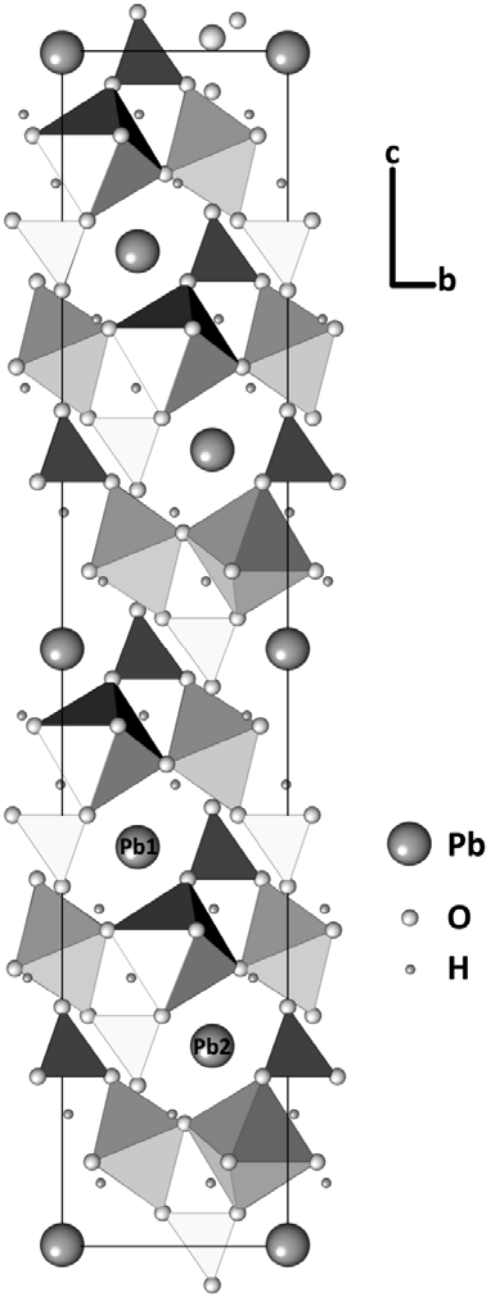

950

951 Fig. 3

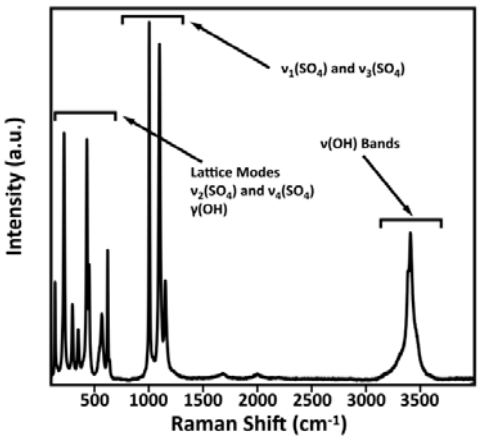

952

953 Fig. 4

954

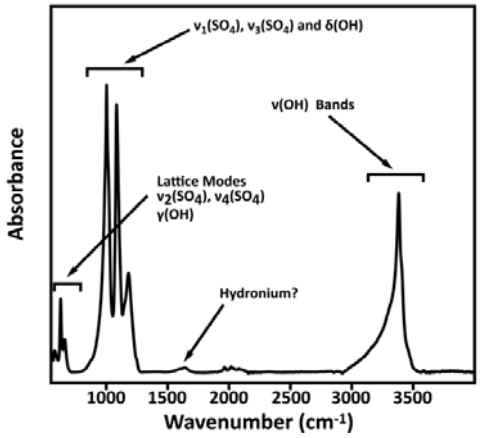

955

956 Fig. 5

957

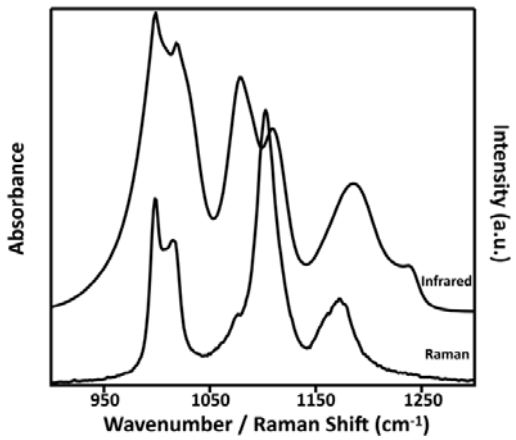

Fig. 6